Seasonal Prediction of the Quasi-Biennial Oscillation

L. Coy[1,2], P. A. Newman[1], A. Molod[1], S. Pawson[1], M. J. Alexander[3], L. Holt[3]

[1]NASA Goddard Space Flight Center, Greenbelt, Maryland

[2]Science Systems and Applications Inc., Lanham, Maryland

[3]Northwest Research Associates, Boulder, Colorado

Key Points:

- A global seasonal forecast system can provide detailed QBO information out to three months.
- EOFs (Empirical Orthogonal Functions) provide a useful basis for QBO forecast comparisons.
- Current QBO forecast biases highlight QBO model deficiencies in need of future improvements.

Corresponding author: Lawrence Coy, `lawrence.coy@nasa.gov`

Abstract

The ability to forecast the Quasi-Biennial Oscillation was examined using Version 2 of NASA's Global Earth Observing System Subseasonal-to-Seasonal (GEOS-S2S) forecasting system. The vertical and time structure of the QBO was characterized by the principal components of the first two empirical orthogonal functions (EOFs). A set of nine-month retrospective forecasts was initialized four times each month between 1981 and early 2019. Validation of 1–9 month forecasts from GEOS-S2S showed that the S2S retrospective QBO forecasts improved skill in predicting the QBO EOF-based amplitude and phase over a simple QBO phase propagation model at forecast lead times of 1–3 months. Results from an initial assessment of whether more accurate QBO forecasts can improve Northern Hemisphere winter sea level pressure forecasts showed no significant forecast improvement at a one month lead time, indicating the need for improved stratosphere-troposphere QBO coupling metrics, pathway identification, and QBO modeling. Overall, these results suggest that future improvements in representing the QBO in global models can increase the skill of 1–3 month QBO forecasts and potentially extend useful QBO forecasts beyond 3 months.

Plain Language Summary

The Quasi Biennial Oscillation (QBO), a switching between westerly and easterly tropical winds in the lower stratosphere ($\sim$18–30 km) with a variable period averaging $\sim$28 months, provides an atmospheric signature with the potential to be predicted months in advance. The period of the QBO is not tied to the solar forcing but rather to the strength of disturbances in the tropical troposphere that then propagate into the stratosphere, leading to a distinctive downward progression of the alternating wind regimes. Since the state of the QBO has been correlated with atmospheric features both in and outside of the tropics and in both the stratospheric and troposphere, improved QBO prediction may lead to improvements in global prediction. The work presented here extends earlier studies based on prediction of the QBO at a single stratospheric level by examining the potential for forecasting the evolving QBO vertical structure and period. Results show that on average the QBO forecasts are useful out to 3 months as they continue to exceed the skill of a simple extrapolation of the QBO at that time.

1 Introduction

The Quasi-Biennial Oscillation (QBO) provides a fascinating example of a long period ($\sim$28 months) atmospheric oscillation not tied to the seasonal cycle. First documented by Ebdon (1960) and Reed et al. (1961) the zonal mean zonal wind shear in the tropical lower stratosphere propagates downward in response to wave driving creating alternating easterly and westerly flow (Holton & Lindzen, 1972). Andrews et al. (1987) and Baldwin et al. (2001) review the structure and theory of the QBO in detail.

Correlations of the QBO with high-latitude surface pressure patterns such as the Arctic Oscillation (AO, Marshall & Scaife, 2009), North Atlantic Oscillation (NAO, Smith et al., 2016) and tropical precipitation modulated by the Madden-Julian Oscillation (MJO, Marshall et al., 2017; Zhang & Zhang, 2018; Wang et al., 2018) create potential for the QBO to provide sub-seasonal to seasonal forecasting guidance in predicting some aspects of the AO, NAO, and MJO (Scaife et al., 2014). The influence of the QBO on the stratospheric polar vortex (Garfinkel et al., 2018; Gray et al., 2018) also creates the potential for improved sub-seasonal to seasonal forecasting of the polar vortex. As shown by Scaife et al. (2014), the quasi-regularity of the QBO period provides a first order, single level (30 hPa), forecast of the QBO tropical lower stratospheric winds based on the average QBO period alone. However, as noted by Scaife et al. (2014), predicting the QBO variability in period, amplitude, and vertical structure requires the forecast model to realistically capture the physics of the QBO.

A comprehensive multi-model examination of the ability to forecast the QBO throughout the QBO vertical domain by Stockdale et al. (2020) revealed high skill in predicting the phase of the QBO out to 6 months at 30 hPa and generally good skill out to 9–12 months both above and below the 30 hPa level. However, the QBO amplitude proved more difficult to predict with a westerly bias at 30 hPa common to all the models and the amplitude of the QBO signal in most models decreasing with time at both 20 and 50 hPa. These results highlighted the potential of current QBO models to forecast the QBO phase and vertical structure out to 6–12 months.

Here we examine the ability of the NASA Global Earth Observing System (GEOS) Sub-seasonal to Seasonal (S2S) forecasting system to forecast the QBO vertical structure and descent rate. This expands on the study of Scaife et al. (2014), where the QBO was characterized solely by the zonal wind at 30 hPa, by considering the QBO evolu-

tion as diagnosed by the first two Empirical Orthogonal Functions (EOFs, Wallace et al., 1993). The EOFs used here provide a consistent evaluation framework for the 9-month forecasts, the Modern-Era Retrospective analysis for Research and Applications, Version 2 (MERRA-2) validation, and a simple, 28-month period based, phase propagation model (PPM). The goal here is to determine whether GEOS-S2S can provide detailed and accurate QBO information in 1–9 month forecasts.

The plan of the paper is as follows: Section 2 describes the forecast model, the validation reanalysis, the EOF calculation, and the EOF based phase propagation model; Section 3 presents the evaluation of the 9-month S2S forecasts when compared to the phase propagation model and MERRA-2; Section 4 discusses some of the features and limitations of the S2S QBO representation; and Section 5 summarizes the results.

2 Forecast and analysis systems

2.1 Forecast system

The nine month retrospective forecasts used to examine QBO forecasting were produced by version 2 of GEOS-S2S (hereafter S2S, Molod et al., 2020). S2S is based on the cubed-sphere dynamical core (Putman & Suarez, 2011), and includes a two moment cloud microphysics module (Barahona et al., 2014), and the cryospheric components of Cullather et al. (2014). The atmosphere model is run at $\sim$ 50km horizontal resolution with 72 vertical levels having $\sim$ 1km vertical resolution in the stratosphere. The eta-coordinate model levels are the same as in the MERRA-2 system and are constant in the stratosphere with 14 levels between 100 and 10 hPa (100.5, 85.4, 72.6, 61.5, 52.0, 43.9, 37.0, 31.1, 26.1, 21.8, 18.1, 15.0, 12.5, and 10.3 hPa). The Modular Ocean Model-5 (Griffies, 2012) is run at approximately $\sim$ 50km resolution. The retrospective forecasts were initialized using MERRA-2 atmospheric reanalysis (Gelaro et al., 2017) and the GMAO S2S Ocean Analysis. Retrospective forecasts are produced from four initial states taken at 5-day intervals in the second half of each month (approximately days 15, 20, 25, and 30). A complete description of the S2S system is found in Molod et al. (2020).

An important aspect of S2S for this study is the ability of the atmospheric model component to represent the QBO. The QBO in S2S is forced mainly by the non-orographic gravity wave drag (GWD) parameterization. This parameterization specifies a discrete wave phase speed spectrum acting as a time independent wave forcing at 400 hPa, where

the latitude dependence of the wave forcing amplitude is tuned to produce a modeled QBO similar to observations (Molod et al., 2015). The vertical propagation and dissipation in the parameterization follow Lindzen (1981) as described in Garcia and Solomon (1985). This parameterization produces a QBO consistent with the original QBO mechanism of Lindzen and Holton (1968).

A large suite of retrospective S2S forecasts have been completed beginning in 1981 that are the basis of the present study. The forecasts were initialized four times each month starting in 1981 and continuing through to the first 11 forecasts (two plus months) of 2019 yielding a total 1,835 forecasts. Each of these forecasts are treated independently for calculation of forecast skill as averaging the four monthly initial dates as an ensemble did not significantly modify the results. For each nine-month retrospective forecast the monthly averaged, zonally averaged, mean wind tendencies were archived on 48 standard pressure levels including 100, 70, 50, 40, 30, 20, and 10 hPa, enabling good vertical resolution over the QBO domain. These tendencies, initialized with the corresponding MERRA-2 wind field, were integrated to generate wind fields at monthly intervals. These in turn were averaged from 10°S–10°N to capture the forecasted tropical zonal wind signature. The tendencies were used in the study because they were saved at higher vertical resolution than the wind field.

2.2 MERRA-2

The MERRA-2 reanalysis (Gelaro et al., 2017; Coy et al., 2016) was used to validate the forecasts. The ongoing MERRA-2 reanalysis, begun in 1980, currently provides 41 years of the QBO signal based on radiosonde and satellite observations combined with the atmospheric model. The MERRA-2 modeled QBO uses the same gravity wave drag (GWD) parameterization as the S2S system described above (see Molod et al., 2015). The MERRA-2 QBO is compared to the QBO in other reanalyses in Kawatani et al. (2016).

The MERRA-2 zonal wind fields taken from model level files (GMAO, 2015) at 00, 06, 12, and 18 UTC were time averaged and then zonally averaged to create a daily time series of zonally average zonal winds from 1 January 1980 through 28 February 2019. The zonal mean winds were then averaged in latitude from 10°S–10°N. The eta-coordinate model levels are the same as in the S2S model with 14 levels between 100 and 10 hPa providing excellent vertical resolution in the QBO domain.

2.3 QBO EOFs

It has been shown that the QBO vertical structure can be well represented by the first two empirical orthogonal functions (EOFs) with the QBO time evolution described by their corresponding two principal components (PCs, Wallace et al., 1993; Fraedrich et al., 1993). While Scaife et al. (2014) represented the QBO by the zonal mean zonal wind at 30 hPa, here we include QBO vertical structure by considering the first two EOFs.

For MERRA-2, the daily equatorial zonal mean zonal winds over the years 1983–2014 and covering the 100–10 hPa (14 model levels) vertical domain were expanded in terms of 14 EOFs as:

$$U(z,t) = \sum_{k=1}^{14} PC_k(t) \cdot EOF_k(z) \tag{1}$$

with the PCs given by:

$$PC_k(t) = \sum_{m=1}^{14} U(z_m,t) \cdot EOF_k(z_m) \tag{2}$$

where $U(z,t)$ is the zonal mean zonal wind averaged over 10°S–10°N. The 14 model levels provide a more spatially even and denser vertical level distribution than studies based on manditory pressure levels. To calculate the EOFs the day-of-year averages were first subtracted from the time series to remove the mean, annual, and semi-annual cycles. Then the 14x14 vertical correlation matrix was constructed from the daily average zonal mean zonal wind fields. Finally, the 14 normalized EOFs were calculated as eigenvectors of the correlation matrix. The first two EOFs explain approximately 94% of the variance of the zonal wind field (Wallace et al., 1993; Fraedrich et al., 1993). Note that the downward propagating QBO signal requires two EOFs, similar in magnitude but approximately 90° out of phase, to represent it. Hereafter we will consider only the first two PC components.

The first two PC components (PC_1 and PC_2) can also be expressed as an amplitude and phase:

$$Amplitude = \sqrt{PC_1^2 + PC_2^2} \tag{3}$$

$$Phase = \arctan(PC_2/PC_1) \tag{4}$$

Differentiating the phase with respect to time yields the QBO descent rate. Note that in this formulation the QBO amplitude, in ms^{-1}, depends on the number of vertical levels used in the calculation of the EOFs as the PC values are vertical sums over the projection of the wind profile on the EOF profile (Equ. 2).

The PC representation of the MERRA-2 QBO from January 1980 through January 2021 (Fig. 1) illustrates the generally circular patten created as the PC components oscillate with time. The 2015 and 2020 QBO disruption events (Newman et al., 2016; Osprey et al., 2016; Tweedy et al., 2017; Saunders et al., 2020; Anstey et al., 2021) are highlighted along with the corresponding prior years. These recently occurring QBO disruptions provide a special forecast challenge.

Because the S2S output are saved on only seven levels, as noted above, these were interpolated to the MERRA-2 levels before being projected onto the MERRA-2 derived EOF vertical structures (Equ. 2) to obtain their corresponding PCs.

2.4 Phase propagation model

To be useful, forecasts based on a dynamical model should improve forecast skill over climatology. However, the uniqueness of the propagating QBO prohibits the use of a typical "annual cycle" climatology: a prediction must be used that is based on the typical propagation of the QBO, initialized by the current QBO state. The simplest QBO prediction estimate consists of a sine wave having the mean QBO period with the phase set by the initial time (Scaife et al., 2014), extrapolating the initial phase of the QBO at a selected level forward in time using an average QBO period. Here we use a more detailed extrapolation based on the average of the MERRA-2 QBO PCs 1 and 2 as described in Appendix 2.4. We refer to this extrapolation, based on the MERRA-2 QBO climatology, as the phase propagation model (PPM), though the model predicts both the QBO amplitude and phase.

The PPM sets the initial EOF based QBO amplitude and phase (PCs 1 and 2) by the initial MERRA-2 PCs and then determines the amplitude and phase at all later times. It includes the average QBO amplitude variation as a function of QBO phase and the average QBO phase variation as a function of the annual cycle allowing the observed slowing descent (lack of phase progression) of the QBO during periods of active extra-tropical planetary wave activity (Wallace et al., 1993; Coy et al., 2020). Using this PPM sets a high bar for the S2S system forecasts.

As an example, the January 1980 initialized PPM's predicted PCs 1 and 2 (Fig. 2) track the MERRA-2 PCs closely for ∼6 years during a time when the QBO cycles were nearly uniform (1980–1986), however when the QBO cycle lengthens (1986-1987), the

PPM is not able to match it (Figs. 2a and b). The square root of the sum of the squares of the differences between the phase propagation forecast and MERRA-2 principal components (Fig. 2c), that is, the magnitude of the vector distance between the forecast and the MERRA-2 QBO in the principal component plane, provides a convenient measure of the forecast error. Visually, good agreement between the forecast and MERRA-2 in Figs. 2a and b occurs when this error value remains below ∼20–25 m/s in the 14 level EOF space. We use this same forecast error quantity when evaluating the S2S 9 month forecasts against MERRA-2.

The PPM's forecast error growth varies greatly depending on the regularity of the QBO after the initial time. For example, the forecast error for the January 1986 initialized phase propagation model rapidly increases above ∼20 m/s in less than half a year (Fig. 3). On average, the mean PPM's forecast error growth with respect to MERRA-2, based on monthly initializations for 1980–2018 (Fig. 4), exceeds 20 m/s after ∼ 1/2 year, so over this time period, the phase propagation forecast is limited to less than one year. However, the broad standard deviation shown in Fig. 4 indicates that a valid PPM forecast can sometimes persist for several years as in Fig. 2.

While the PPM was initialized monthly from 1980–2018 in this section, in the following section the PPM will be initialized on exactly the same dates as the S2S initial dates.

3 Forecast evaluation

Forecast errors evaluated for the 1,835 9-month S2S QBO forecasts, represented by PCs 1 and 2 and validated against the MERRA-2 PCs, yield the corresponding mean forecast error growth for the S2S system (Fig. 5). Each point in Fig. 5 denotes the error derived from S2S forecast profiles projected onto the MERRA-2 EOFs at one month intervals. As with the PPM, the mean and standard deviation of the S2S forecast errors increase with increasing forecast length. However, the monthly mean and median error values at 1–4 months forecast time for S2S remain smaller than those of the PPM, indicating improvement of the dynamically based S2S forecast over the statistically based PPM result. At longer forecast lead times the mean S2S error becomes greater than the PPM results, possibly because of systematic differences between the S2S modeled and

MERRA-2 analyzed QBO vertical structure along with the greater variability of the S2S than the PPM (see section 4 below).

Consistent with the forecast error growth, the percentage of forecasts with forecast errors remaining less than 20 m/s at each forecasted month (Fig. 6) reveals the advantage of S2S over the PPM at forecast lengths of 2 and 3 months with about an equal chance of a successful forecast at 4 months. As expected from Fig. 5, the longer, 5–9 month forecasts, favor the PPM results. Random selection of half the forecasts leads to essentially the same results as denoted by the relatively small error bars in Fig. 6. However, examination of continuous, more limited, time periods alters these results. As a specific example, simply dividing the 1981-2018 time period into first and second halves reveals relatively unchanged S2S performance in both halves compared with the PPM changes, resulting in improved performance of S2S over the PPM in the second half. Nevertheless the S2S percentage curve changes when other time periods are selected. Merely stopping the second half early, at 2014, to avoid the first QBO disruption, improves the performance of both the S2S and PPM system (not shown).

The same forecast error parameter (error less than 20 m/s) can be sorted by the initial condition (Fig. 7). Initialization with larger than average QBO amplitudes improves the three month forecasts. The three month forecasts are also more skillful when initialized in June, July, August. This result differs from the relatively poor August start results shown in Scaife et al. (2014). Most striking is the dependence of the forecast skill on the initial phase of the QBO with the easterly and westerly phases having a higher percentage of good forecasts than the transition seasons.

As noted in the introduction, the QBO influences tropospheric weather such as the NAO (Gray et al., 2018). Here we present a preliminary investigation into the question of whether having accurate QBO forecasts improves tropospheric sea level pressure (SLP) forecasting. The MERRA-2 NH winter mean SLP is correlated with phase of the stratospheric QBO. Fig. 8 shows the December through February mean SLP composted by the sign of the anomaly in the 30 hPa equatorial zonal mean winds averaged over the same 3-months. Based on Fig. 8 we chose the SLP difference between 65°N and 45°N at 0° longitude as a single, a priori chosen, variable to represent the NAO. For this SLP difference variable, the S2S retrospective forecast correlated most strongly with MERRA-

2 during January, February, and March at one month lead times, with correlations between 0.3 and 0.4 (Fig. 9). Correlations at longer forecast lead times were near zero.

Sorting the forecasts by their one month S2S QBO forecast error relative to the median error value, divides the forecasts into equally sized "good" and "bad" QBO forecast groups, though at one month lead time most of the QBO forecast errors remain relatively small. The SLP correlation between the S2S forecast and MERRA-2 increases for the more accurate QBO forecasts in January, however the opposite result occurs for both February and March QBO forecasts (Fig. 9). The standard deviations of correlations based on the random selection of QBO forecasts provide a measure of the significance of the sorted correlations. Since the sorted correlations vary, at best, only one random correlation standard deviation, the more accurate prediction of the QBO failed to improve the corresponding SLP/NAO forecasts.

4 S2S QBO diagnostics

Basing the S2S forecast validation on EOF structures enables the identification of some of the current GEOS-S2S modeled QBO's strengths and weaknesses.

The average descent rate of the QBO (Fig. 10a) agrees well with the MERRA-2 value at all forecast lead times, indicating that S2S correctly models the average QBO period. However, the differences between S2S and MERRA-2 variability in the descent rate (Fig. 10b) indicates that the S2S forecast model QBO, constrained by the fixed parameterized gravity wave forcing, lacks some of the observed variability in QBO period. Based on the consistency of the descent, and hence period, the S2S system should provide useful forecasts of the QBO phase only, on average, at nine months, similar to the single level predictability found in Scaife et al. (2014).

The S2S QBO amplitude (Fig. 10c) significantly underestimates the QBO amplitude as forecast lead time increases, indicating either weak forecasted QBO winds or a mismatch with the observed QBO vertical structure. This result is consistent with the forecasted amplitude decrease seen in many of the models examined in Stockdale et al. (2020). As it is standard practice to consider seasonal forecast results with respect to the known forecast model bias, this amplitude bias was subtracted from the S2S QBO amplitude in computing the forecast error differences with MERRA-2 presented in Figs. 6 and 5. While this bias removal, on average, helps the S2S QBO forecasts to better match

the EOF vertical structures it should be noted that it probably will not aid in relating the QBO to features outside of the QBO domain. That is, it is nevertheless important to develop models with unbiased QBO structures. Finally, the S2S amplitude variability corresponds closely to the MERRA-2 amplitude variability with no dependence on forecast lead time (Fig. 10d).

Comparing a series of S2S 9 month forecasts of the QBO winds with MERRA-2 (Fig. 11) illustrates some aspects of the mismatch in vertical structure. The S2S system forecasts the QBO period closely, however the forecasted westerlies fail to descend to 100 hPa in 2013–14 and hence, they project poorly onto the MERRA-2 EOF structures at the 9-month forecast lead time. A detailed examination of the QBO in thirteen general circulation models (Bushell et al., 2020) found QBO amplitudes generally too weak over the 50–70 hPa altitude range, with the maximum amplitude shifted to 10 hPa, consistent with the S2S results. Bushell et al. (2020) also found weak QBO easterly winds in most models, once again, consistent with the weak S2S easterlies seen in Fig. 11b. In addition, the S2S 9 month forecasts fail to capture the QBO disruption of 2015–16 (Newman et al., 2016; Osprey et al., 2016; Tweedy et al., 2017). Other systematic S2S forecast biases, such as the westerlies that develop in the upper troposphere, potentially affect vertical wave propagation, both resolved and parameterized, and in turn possibly lead to a poorer representation of the 9-month QBO forecasts.

Examination of specific S2S forecasts, represented by EOFs 1 and 2 (Fig. 12), illustrate the difficulty in capturing the future QBO, especially when the EOF amplitudes become unusually small, along with successful forecasts during more typical QBO cycles. In 1988 (Fig. 12a) the smallness of the MERRA-2 analysis-based QBO amplitude (blue curve) indicates a poor fit of its vertical zonal wind profile to the EOF 1 pattern. Beginning from the MERRA-2 initial condition, the S2S forecast (red curve) decreases in amplitude for the first months of the forecast (as in the analysis) before following a more typical QBO phase propagation at the reduced, nearly constant, amplitude thereby maintaining a fairly good 9-month QBO forecast. The corresponding PPM forecast (black curve) maintains amplitude but propagates more slowly than the MERRA-2 analysis or S2S forecast.

For the 11 April 2015 initial condition (Fig. 12b), the 9-month S2S and PPM forecasts both follow the MERRA-2 analysis for $\sim$7-months, however they both fail to cap-

ture the QBO disruption seen in the final two months of the forecast (Jan-Feb 2016). More difficulty is encountered in forecasting from the 20 July 2015 initialization (Fig. 12c) as both the S2S and phase propagation model forecasts miss the 2016 QBO disruption. Furthermore, both S2S and PPM forecasts tend to produce counter-clockwise (downward) QBO phase propagation, even when the observed, disrupted QBO, reversed its phase propagation (Figure 12d). By construction, the PPM always moves the QBO counterclockwise (downward phase propagation) in this EOF space, however, future improvements in the S2S model may allow for more realistic QBO forecasts during such unusual QBO times.

5 Summary and Conclusions

This study examined 1,835 9-month GEOS-S2S global model forecasts of the QBO winds and vertical structure as characterized by the first two QBO EOFs . These S2S retrospective QBO forecasts were found to, on average, improve skill over a simple extrapolated QBO amplitude and phase (PPM) for forecast lead times of 1–3 months. In addition, results suggest that QBO forecast skill depends on the phase of the QBO, with easterly or westerly QBO initial conditions improving skill over the transition season. A measure of forecast error based on amplitude and phase replaced other measures, such as correlation coefficients, capturing forecasted variations in QBO vertical structure, not just a mean phase change. Using the EOF description in conjunction with the PPM for forecast evaluation yielded a shorter QBO prediction lead time than found in previous studies, such as Scaife et al. (2014) and Stockdale et al. (2020). How much detail is needed for a QBO forecast to be useful will depend on the particular application.

These S2S QBO forecast results also reveal some features and limitations of the QBO representation in the current S2S model. The S2S forecasted average QBO downward phase propagation (reflecting the mean QBO period) and QBO amplitude variability agreed well with MERRA-2 (Fig. 10a and d). However, the low S2S phase variability (QBO period variability) compared to MERRA-2 and the systematic S2S amplitude decrease with forecast lead time suggests areas where the forecasted QBO needs improvement (Fig. 10b and c).

Examination of individual forecasts during and after the 2015–16 QBO disruption illustrates some additional limitations of the current model QBO parameterization (Figs. 12b,

c, and d). While the global model results of Watanabe et al. (2018) successfully forecast the 2015–16 QBO disruption at about one month lead time, the forecasting of the QBO disruption several months ahead likely remains difficult as it would require the forecasting of the highly variable middle latitude Rossby waves and their equatorial propagation (Osprey et al., 2016; Coy et al., 2017). However, the propagation of the post-disruption QBO during early 2016 results from more typical equatorial wave forcing so that forecasting the unusual upward and more typical downward propagation of the additional, disrupted, QBO wind shears is perhaps a realistic model development goal.

A complete representation of the disrupted QBO requires the consideration of higher order EOFs such as EOFs 3 and 4 that together represent the behavior of an additional wind shear region in the QBO domain (Fig. 13). During the disruptions of 2016 and 2020 the amplitude of EOFs 3 and 4 increased, accompanied by only a slight clockwise change in phase (upward shear propagation) as the disrupting middle latitude waves created an anomalous wind shear region. Once formed these additional wind shears propagated steadily downward (counterclockwise phase progression in Fig. 13) suggesting that global models with improved representation of vertically propagating equatorial waves may possibly capture the evolution of these post-disruption shears.

An initial assessment of whether more accurate QBO forecasts improve tropospheric SLP forecasts showed no significant results at a 1-month lead time. This result is consistent with the multi-model results of Butler et al. (2016) that show a weak NH response to the QBO phase. In addition to improving the QBO forecast, other aspects of the global circulation need to be realistically coupled to the QBO to fully characterize the relation between the QBO and SLP, a topic beyond the scope of this paper. A better understanding of the physical mechanisms relating the QBO to SLP may be needed to properly evaluate potential forecast skill improvements in this area.

This study shows that with present-day GWD codes (and overall model formulation), the QBO can be predicted from a good initial state with some skill out to three months, but beyond that the complex Earth system model does no better than the PPM. One factor that limits the current skill in predicting the vertical structure is the lack of descent of the QBO to 100 hPa, a common problem with current QBO simulations, that likely requires additional development of the parameterized GW code and improvements in vertical resolution (Geller et al., 2016; Garfinkel et al., 2021). Correcting the verti-

cal structure should improve the forecast bias seen in the amplitude (Fig. 10c). In addition, planned development of the S2S GW parameterization will couple the waves to the model convection and this can be expect to address the low S2S QBO period variability (Fig. 10b). While forecasting QBO disruption events themselves may remain problematic, tuning of the parameterized GW spectrum has the potential to capture the behavior of the additional wind shears seen after the disruptions, leading to improved forecasts during those times.

One way to summarize the results here is that specified GW forcing (S2S) improves over the specified QBO period (PPM), at least out to three months when evaluated in terms of EOF-based amplitude and phase. This suggests that the S2S forecasts benefit from the non-linearity contained in the QBO's wave-mean flow interaction that is missing from the PPM. Accurately modeling this non-linear, wave-mean flow interaction is key to improving QBO forecasts

Overall, these results show the ability of current global models to successfully provide detailed QBO forecast information out to three months, with over 75% of the forecasts in this study considered to be accurate at the end of three months (Fig. 6). However, this study also reveals areas where models can improve the representation of the QBO, such as the descent of the QBO to 100 hPa and the propagation of wind shears during QBO disruption events. With model improvements it may be possible to both increase the accuracy of the one-three month forecasts and extend the QBO forecasts beyond three months.

Appendix A QBO Phase Propagation Model

This section describes the EOF based QBO phase propagation model and follows closely the QBO prediction model described in Wallace et al. (1993). Rather than using a fixed frequency for the QBO cycle, this model incorporates the climatological signal of the known slowing of the QBO descent during periods of planetary wave activity (Coy et al., 2020) into the QBO phase propagation. The QBO frequency ω can be expanded over the annual cycle as a Fourier cosine and sine series:

$$\omega = a_0 + \sum_{k=1}^{k_{max}} [a_k \cos(k\omega_a t) + b_k \sin(k\omega_a t)] \tag{A1}$$

where t is time, ω_a is the annual frequency, a_0 is the mean QBO frequency, and a_k and b_k are higher harmonics calculated from the average MERRA-2 annual cycle in QBO fre-

quency. Using a k_{max} of 2 is enough to capture the annual and semi-annual variability of interest. The QBO phase, ϕ, can then be determined by integrating ω with respect to time:

$$\phi(t) = \phi_0 + a_0(t - t_0) + \sum_{k=1}^{k_{max}} \frac{1}{k\omega_a} \left[a_k \sin(k\omega_a t) - b_k \cos(k\omega_a t)\right] \Big|_{t_0}^{t} \qquad \text{(A2)}$$

where ϕ_0 is the initial QBO phase and t_0 is the initial time.

Rather than using a fixed QBO amplitude, the predicted QBO amplitude can be constructed to reflect the known amplitude variation as a function of EOF based QBO phase. In terms of the propagated phase above (Equ. A2), the average QBO EOF amplitude, A_{EOF} is expanded as:

$$A_{EOF}(t) = c_0 + \sum_{j=1}^{j_{max}} \left[c_j \cos(j\phi) + d_j \sin(j\phi)\right] \qquad \text{(A3)}$$

where c_0, c_j and d_j are determined from the MERRA-2 mean EOF QBO amplitude as a function of the QBO phase over the QBO cycle. A j_{max} of 1 or 2 captures most of the variability. The initial amplitude, A_0, can be incorporated as a decay to A_{EOF}:

$$A(t) = (A_0 - A_{EOF})e^{-(t-t_0)/T} + A_{EOF} \qquad \text{(A4)}$$

where A is the propagated amplitude and T is a decay to the EOF amplitude timescale, taken in this study to be one year.

Acknowledgments

This work was supported by the NASA Modeling and Analysis Program and the NASA Atmospheric Composition Modeling and Analysis Program. Computer resources supporting this work were provided by the NASA High-End Computing (HEC) Program through the NASA Center for Climate Simulation (NCCS) at Goddard Space Flight Center. The MERRA-2 assimilated products are available from the NASA GES DISC collection (`https://disc.gsfc.nasa.gov/datasets/M2I3NVASM_5.12.4/summary`). GEOS-S2S forecast output products are available at `https://gmao.gsfc.nasa.gov/gmaoftp/gmaofcst/` and the file specification document for GEOS-S2S is available online (`https://gmao.gsfc.nasa.gov/pubs/docs/Nakada1033.pdf`). Selected GEOS-S2S fields used in this study are at `https://gmao.gsfc.nasa.gov/gmaoftp/larrycoy/geos_s2s_v02/` The authors wish to sincerely thank both reviewers for their close reading and insightful comments that resulted in significant improvements to this work.

References

Andrews, D. G., Holton, J. R., & Leovy, C. B. (1987). *Middle atmosphere dynamics.* Academic Press.

Anstey, J., Banyard, T., Butchart, N., Coy, L., Newman, P. A., Osprey, S., & Wright, C. (2021). Prospect of increased disruption to the QBO in a changing climate. *Geophys. Res. Lett., submitted*.

Baldwin, M. P., Gray, L. J., Dunkerton, T. J., Hamilton, K., Haynes, P. H., Randel, W. J., ... Takahasi, M. (2001). The quasi-biennial oscillation. *Rev. Geophys.*, *39*, 179-229.

Barahona, D., Molod, A., Bacmeister, J., Nenes, A., Gettelman, A., Morrison, H., ... Eichmann, A. (2014). Development of two-moment cloud microphysics for liquid and ice within the NASA Goddard Earth Observing System Model (GEOS-5). *Geoscientific Model Development*, *7*(4), 1733–1766. Retrieved from https://www.geosci-model-dev.net/7/1733/2014/ doi: 10.5194/gmd-7-1733-2014

Bushell, A. C., Anstey, J. A., Butchart, N., Kawatani, Y., Osprey, S. M., Richter, J. H., ... Yukimoto, S. (2020). Evaluation of the Quasi-Biennial Oscillation in global climate models for the SPARC QBO-initiative. *Quarterly Journal of the Royal Meteorological Society*, *n/a*(n/a). Retrieved from https://rmets.onlinelibrary.wiley.com/doi/abs/10.1002/qj.3765 doi: https://doi.org/10.1002/qj.3765

Butler, A. H., Arribas, A., Athanassiadou, M., Baehr, J., Calvo, N., Charlton-Perez, A., ... Yasuda, T. (2016). The climate-system historical forecast project: do stratosphere-resolving models make better seasonal climate predictions in boreal winter? *Quarterly Journal of the Royal Meteorological Society*, *142*(696), 1413-1427. Retrieved from https://rmets.onlinelibrary.wiley.com/doi/abs/10.1002/qj.2743 doi: https://doi.org/10.1002/qj.2743

Coy, L., Newman, P. A., Pawson, S., & Lait, L. R. (2017). Dynamics of the disrupted 2015/16 quasi-biennial oscillation. *Journal of Climate*, *30*(15), 5661-5674. Retrieved from https://doi.org/10.1175/JCLI-D-16-0663.1 doi: 10.1175/JCLI-D-16-0663.1

Coy, L., Newman, P. A., Strahan, S., & Pawson, S. (2020). Seasonal variation of the quasi-biennial oscillation descent. *Journal of Geophysical Re-*

search: Atmospheres, *125*(18), e2020JD033077. Retrieved from https://agupubs.onlinelibrary.wiley.com/doi/abs/10.1029/2020JD033077 doi: 10.1029/2020JD033077

Coy, L., Wargan, K., Molod, A. M., McCarty, W. R., & Pawson, S. (2016). Structure and dynamics of the quasi-biennial oscillation in MERRA-2. *J. Clim.*, *29*, 5339-5354. doi: 10.1175/JCLI-D-15-0809.1

Cullather, R. I., Nowicki, S. M. J., Zhao, B., & Suarez, M. J. (2014). Evaluation of the surface representation of the greenland ice sheet in a general circulation model. *Journal of Climate*, *27*(13), 4835-4856. Retrieved from https://doi.org/10.1175/JCLI-D-13-00635.1 doi: 10.1175/JCLI-D-13-00635.1

Ebdon, R. A. (1960). Notes on the wind flow at 50 mb in tropical and sub-tropical regions in January 1957 and January 1958. *Quarterly Journal of the Royal Meteorological Society*, *86*(370), 540-542. Retrieved from https://rmets.onlinelibrary.wiley.com/doi/abs/10.1002/qj.49708637011 doi: 10.1002/qj.49708637011

Fraedrich, K., Pawson, S., & Wang, R. (1993). An EOF analysis of the vertical-time delay structure of the quasi-biennial oscillation. *Journal of the Atmospheric Sciences*, *50*(20), 3357-3365. Retrieved from https://doi.org/10.1175/1520-0469(1993)050<3357:AEAOTV>2.0.CO;2 doi: 10.1175/1520-0469(1993)050⟨3357:AEAOTV⟩2.0.CO;2

Garcia, R. R., & Solomon, S. (1985). The effect of breaking gravity waves on the dynamics and chemical composition of the mesosphere and lower thermosphere. *Journal of Geophysical Research: Atmospheres*, *90*(D2), 3850-3868. Retrieved from https://agupubs.onlinelibrary.wiley.com/doi/abs/10.1029/JD090iD02p03850 doi: 10.1029/JD090iD02p03850

Garfinkel, C. I., Gerber, E. P., Shamir, O., Rao, J., Jucker, M., White, I., & Paldor, N. (2021). A QBO cookbook: Sensitivity of the quasi-biennial oscillation to resolution, resolved waves, and parameterized gravity waves. *Journal of Advances in Modeling Earth Systems*, *n/a*(n/a), e2021MS002568. Retrieved from https://agupubs.onlinelibrary.wiley.com/doi/abs/10.1029/2021MS002568 (e2021MS002568 2021MS002568) doi: https://doi.org/10.1029/2021MS002568

Garfinkel, C. I., Schwartz, C., Domeisen, D. I. V., Son, S.-W., Butler, A. H., &

White, I. P. (2018). Extratropical atmospheric predictability from the quasi-biennial oscillation in subseasonal forecast models. *Journal of Geophysical Research: Atmospheres*, *123*(15), 7855-7866. Retrieved from `https://agupubs.onlinelibrary.wiley.com/doi/abs/10.1029/2018JD028724` doi: 10.1029/2018JD028724

Gelaro, R., McCarty, W., Suarez, M. J., Todling, R., Molod, A., Takacs, L., ... Zhao, B. (2017). The Modern-Era Retrospective Analysis for Research and Applications, Version 2 (MERRA-2). *Journal of Climate*, *30*(14), 5419-5454. Retrieved from `https://doi.org/10.1175/JCLI-D-16-0758.1` doi: 10.1175/JCLI-D-16-0758.1

Geller, M. A., Zhou, T., Shindell, D., Ruedy, R., Aleinov, I., Nazarenko, L., ... Faluvegi, G. (2016). Modeling the QBO–Improvements resulting from higher-model vertical resolution. *Journal of Advances in Modeling Earth Systems*, *8*(3), 1092-1105. Retrieved from `https://agupubs.onlinelibrary.wiley.com/doi/abs/10.1002/2016MS000699` doi: https://doi.org/10.1002/2016MS000699

GMAO. (2015). *Global Modeling and Assimilation Office, inst3 3d asm Nv: MERRA-2 3D Assimilated Meteorological Fields 3-hourly (model level, 0.625x0.5L42), version 5.12.4.* Greenbelt, MD, USA: Goddard Space Flight Center Distributed Active Archive Center (GSFC DAAC). (Accessed March 2019) doi: 10.5067/WWQSXQ8IVFW8

Gray, L., Anstey, J. A., Kawatani, Y., Y., H. L., Osprey, S., & Schenzinger, V. (2018). Surface impacts of the quasi biennial oscillation. *Atmos. Chem. Phys.*, *18*, 8227–8247. doi: https://doi.org/10.5194/acp-18-8227-2018

Griffies, S. M. (2012). *Elements of the modular ocean model (MOM)* (Tech. Rep.). NOAA/Geophysical Fluid Dynamics Laboratory. (Available online at https://mom-ocean.github.io/assets/pdfs/MOM5_manual.pdf)

Holton, J. R., & Lindzen, R. S. (1972). An updated theory for the quasi-biennial cycle of the tropical stratosphere. *Journal of the Atmospheric Sciences*, *29*(6), 1076-1080. Retrieved from `https://doi.org/10.1175/1520-0469(1972)029<1076:AUTFTQ>2.0.CO;2` doi: 10.1175/1520-0469(1972)029⟨1076:AUTFTQ⟩2.0.CO;2

Kawatani, Y., Hamilton, K., Miyazaki, K., Fujiwara, M., & Anstey, J. A. (2016).

Representation of the tropical stratospheric zonal wind in global atmospheric reanalyses. *Atmos. Chem. Phys.*, *16*, 6681-6699. doi: 10.5194/acp-16-6681-2016

Lindzen, R. S. (1981). Turbulence and stress owing to gravity wave and tidal breakdown. *Journal of Geophysical Research: Oceans*, *86*(C10), 9707-9714. doi: 10.1029/JC086iC10p09707

Lindzen, R. S., & Holton, J. R. (1968). A theory of the quasi-biennial oscillation. *Journal of the Atmospheric Sciences*, *25*(6), 1095-1107. doi: 10.1175/1520-0469(1968)025⟨1095:ATOTQB⟩2.0.CO;2

Marshall, A. G., Hendon, H. H., Son, S.-W., & Lim, Y. (2017, Aug 01). Impact of the quasi-biennial oscillation on predictability of the Madden–Julian oscillation. *Climate Dynamics*, *49*(4), 1365–1377. Retrieved from `https://doi.org/10.1007/s00382-016-3392-0` doi: 10.1007/s00382-016-3392-0

Marshall, A. G., & Scaife, A. A. (2009). Impact of the QBO on surface winter climate. *Journal of Geophysical Research: Atmospheres*, *114*(D18). Retrieved from `https://agupubs.onlinelibrary.wiley.com/doi/abs/10.1029/2009JD011737` doi: 10.1029/2009JD011737

Molod, A., Hackert, E., Vikhliaev, Y., Zhao, B., Barahona, D., Vernieres, G., ... Pawson, S. (2020). GEOS-S2S Version 2: The GMAO high resolution coupled model and assimilation system for seasonal prediction. *J. Geophys. Res. Atmos.*. (submitted)

Molod, A., Takacs, L., Suarez, M., & Bacmeister, J. (2015). Development of the GEOS-5 atmospheric general circulation model: Evolution from MERRA to MERRA2. *Geosci. Model Dev.*, *8*, 1339-1356. doi: doi:10.5194/gmd-8-1339-2015

Newman, P. A., Coy, L., Pawson, S., & Lait, L. R. (2016). The anomalous change in the QBO in 2015–2016. *Geophysical Research Letters*, *43*(16), 8791–8797. Retrieved from `http://dx.doi.org/10.1002/2016GL070373` (2016GL070373) doi: 10.1002/2016GL070373

Osprey, S. M., Butchart, N., Knight, J. R., Scaife, A. A., Hamilton, K., Anstey, J. A., ... Zhang, C. (2016). An unexpected disruption of the atmospheric quasi-biennial oscillation. *Science*. doi: 10.1126/science.aah4156

Putman, W. M., & Suarez, M. (2011). Cloud-system resolving simulations with

the NASA Goddard Earth Observing System global atmospheric model (GEOS-5). *Geophysical Research Letters*, *38*(16). Retrieved from https://agupubs.onlinelibrary.wiley.com/doi/abs/10.1029/2011GL048438 doi: 10.1029/2011GL048438

Reed, R. J., Campbell, W. J., Rasmussen, L. A., & Rogers, D. G. (1961). Evidence of a downward-propagating, annual wind reversal in the equatorial stratosphere. *Journal of Geophysical Research (1896-1977)*, *66*(3), 813-818. Retrieved from https://agupubs.onlinelibrary.wiley.com/doi/abs/10.1029/JZ066i003p00813 doi: 10.1029/JZ066i003p00813

Saunders, M. A., Lea, A. S. R., & Smallwood, J. R. (2020). The quasi-biennial oscillation: A second disruption in four years. *Earth and Space Science Open Archive*, 16. Retrieved from https://doi.org/10.1002/essoar.10504326.1 doi: 10.1002/essoar.10504326.1

Scaife, A. A., Athanassiadou, M., Andrews, M., Arribas, A., Baldwin, M., Dunstone, N., … Williams, A. (2014). Predictability of the quasi-biennial oscillation and its northern winter teleconnection on seasonal to decadal timescales. *Geophysical Research Letters*, *41*(5), 1752–1758. Retrieved from http://dx.doi.org/10.1002/2013GL059160 (2013GL059160) doi: 10.1002/2013GL059160

Smith, D. M., Scaife, A. A., Eade, R., & Knight, J. R. (2016). Seasonal to decadal prediction of the winter North Atlantic Oscillation: emerging capability and future prospects. *Quarterly Journal of the Royal Meteorological Society*, *142*(695), 611-617. Retrieved from https://rmets.onlinelibrary.wiley.com/doi/abs/10.1002/qj.2479 doi: 10.1002/qj.2479

Stockdale, T. N., Kim, Y.-H., Anstey, J. A., Palmeiro, F. M., Butchart, N., Scaife, A. A., … Yukimoto, S. (2020). Prediction of the quasi-biennial oscillation with a multi-model ensemble of qbo-resolving models. *Quarterly Journal of the Royal Meteorological Society*, *n/a*(n/a). Retrieved from https://rmets.onlinelibrary.wiley.com/doi/abs/10.1002/qj.3919 doi: https://doi.org/10.1002/qj.3919

Tweedy, O. V., Kramarova, N. A., Strahan, S. E., Newman, P. A., Coy, L., Randel, W. J., … Frith, S. M. (2017). Response of trace gases to the disrupted 2015–2016 quasi-biennial oscillation. *Atmospheric Chemistry and Physics*, *17*(11),

6813–6823. Retrieved from https://www.atmos-chem-phys.net/17/6813/2017/ doi: 10.5194/acp-17-6813-2017

Wallace, J. M., Panetta, R. L., & Estberg, J. (1993). Representation of the equatorial stratospheric quasi-biennial oscillation in EOF phase space. *Journal of the Atmospheric Sciences*, *50*(12), 1751-1762. Retrieved from https://doi.org/10.1175/1520-0469(1993)050<1751:ROTESQ>2.0.CO;2 doi: 10.1175/1520-0469(1993)050⟨1751:ROTESQ⟩2.0.CO;2

Wang, J., Kim, H.-M., Chang, E. K. M., & Son, S.-W. (2018). Modulation of the MJO and North Pacific storm track relationship by the QBO. *Journal of Geophysical Research: Atmospheres*, *123*(8), 3976-3992. Retrieved from https://agupubs.onlinelibrary.wiley.com/doi/abs/10.1029/2017JD027977 doi: 10.1029/2017JD027977

Watanabe, S., Hamilton, K., Osprey, S., Kawatani, Y., & Nishimoto, E. (2018). First successful hindcasts of the 2016 disruption of the stratospheric quasi-biennial oscillation. *Geophysical Research Letters*, *45*(3), 1602-1610. Retrieved from https://agupubs.onlinelibrary.wiley.com/doi/abs/10.1002/2017GL076406 doi: https://doi.org/10.1002/2017GL076406

Zhang, C., & Zhang, B. (2018). QBO-MJO connection. *Journal of Geophysical Research: Atmospheres*, *123*(6), 2957-2967. Retrieved from https://agupubs.onlinelibrary.wiley.com/doi/abs/10.1002/2017JD028171 doi: 10.1002/2017JD028171

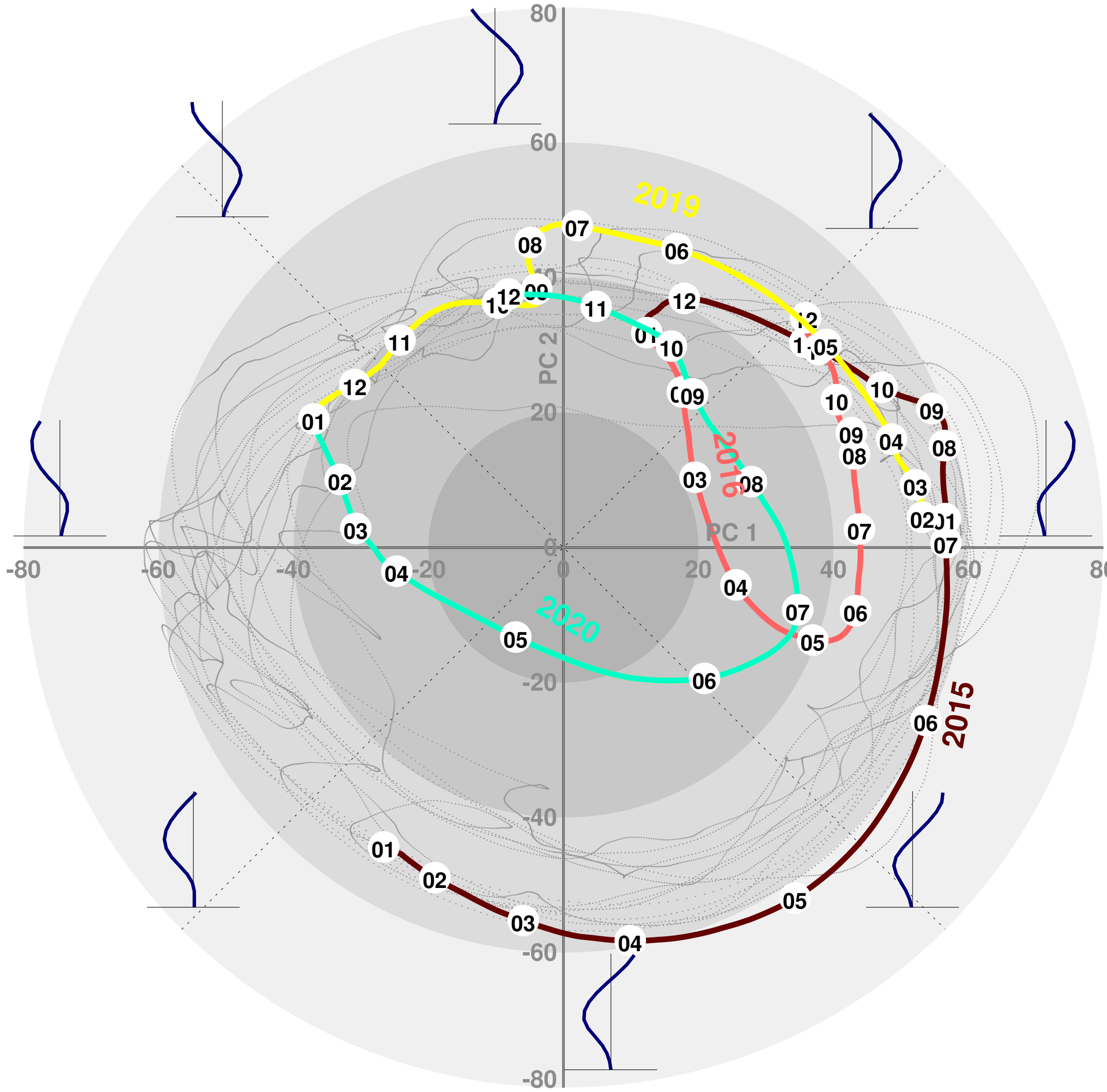

Figure 1. PC1 vs PC2 for MERRA-2. The gray dots are daily values from January 1980 through January 2021. The years 2015, 2016, 2019, 2020 are highlighted brown, red, yellow, cyan respectively. The numbers in the white circles denote the first day of the numbered month. The EOF structures are illustrated at the appropriate phases with the EOF 1 on the right and EOF 2 on the top. The amplitudes on the axes are calculated as a sum of the EOF projection over the 14 vertical levels from 100–10 hPa. The EOFs are based on MERRA-2 winds from January 1980 through December 2014.

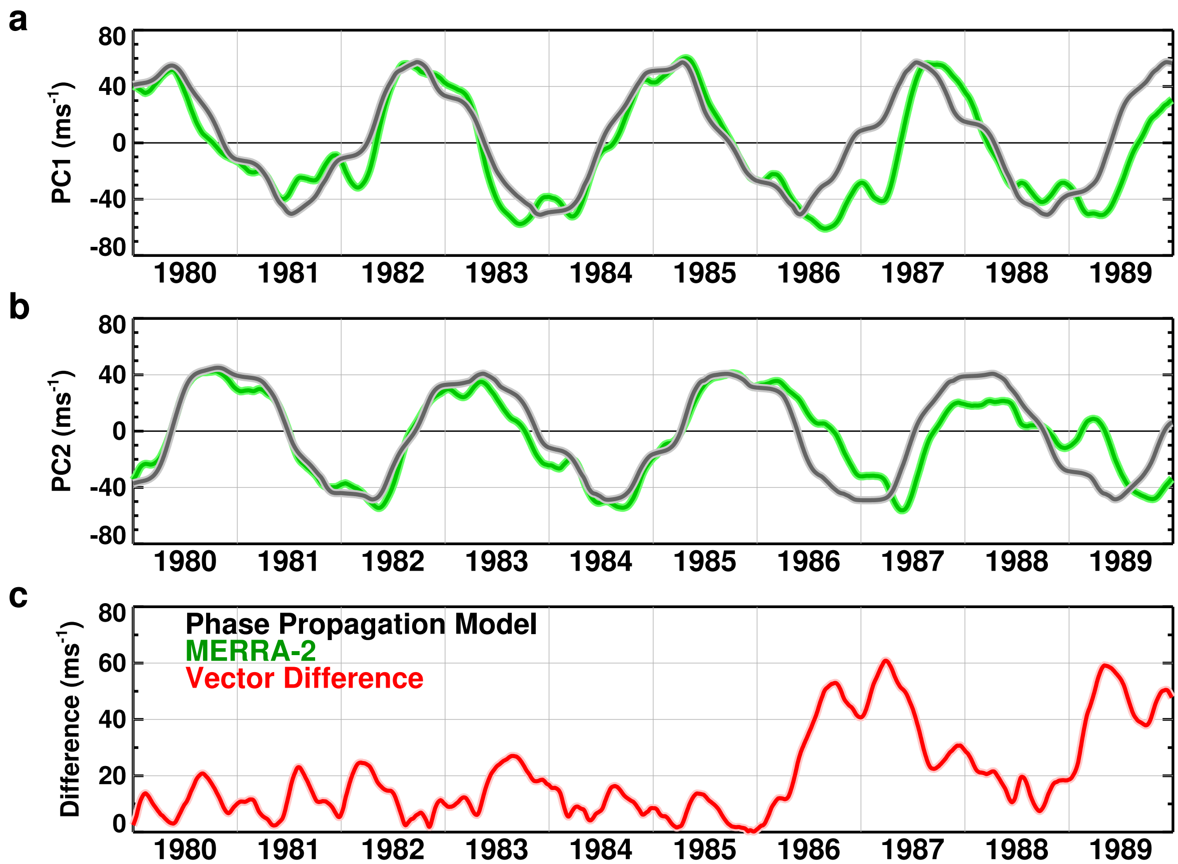

Figure 2. Ten year phase propagation forecast initialized on 1 January 1980 compared to MERRA-2 (green curves) for a) PC1 and b) PC2, along with c) the vector amplitude difference between the phase propagation model and MERRA-2 as a function of year.

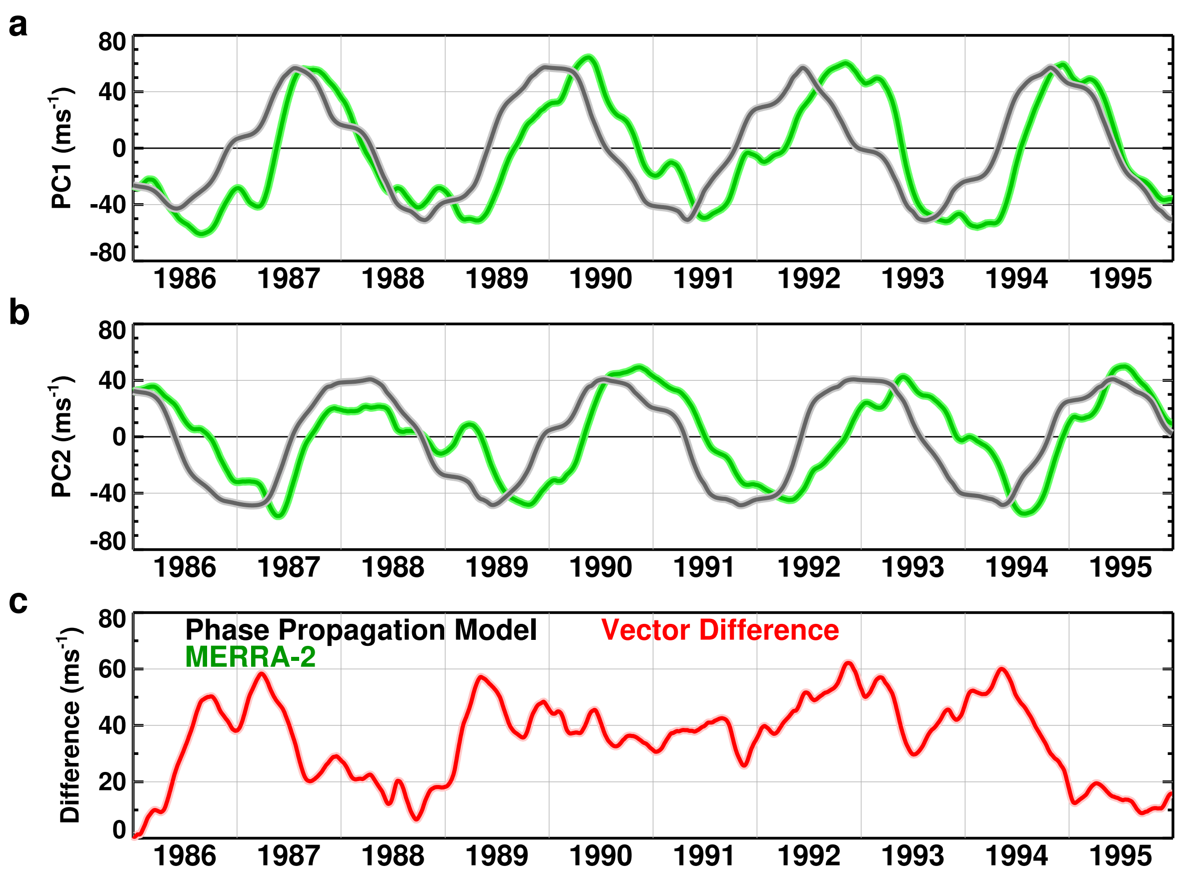

Figure 3. Same as Fig. 2 except initialized on 1 January 1986.

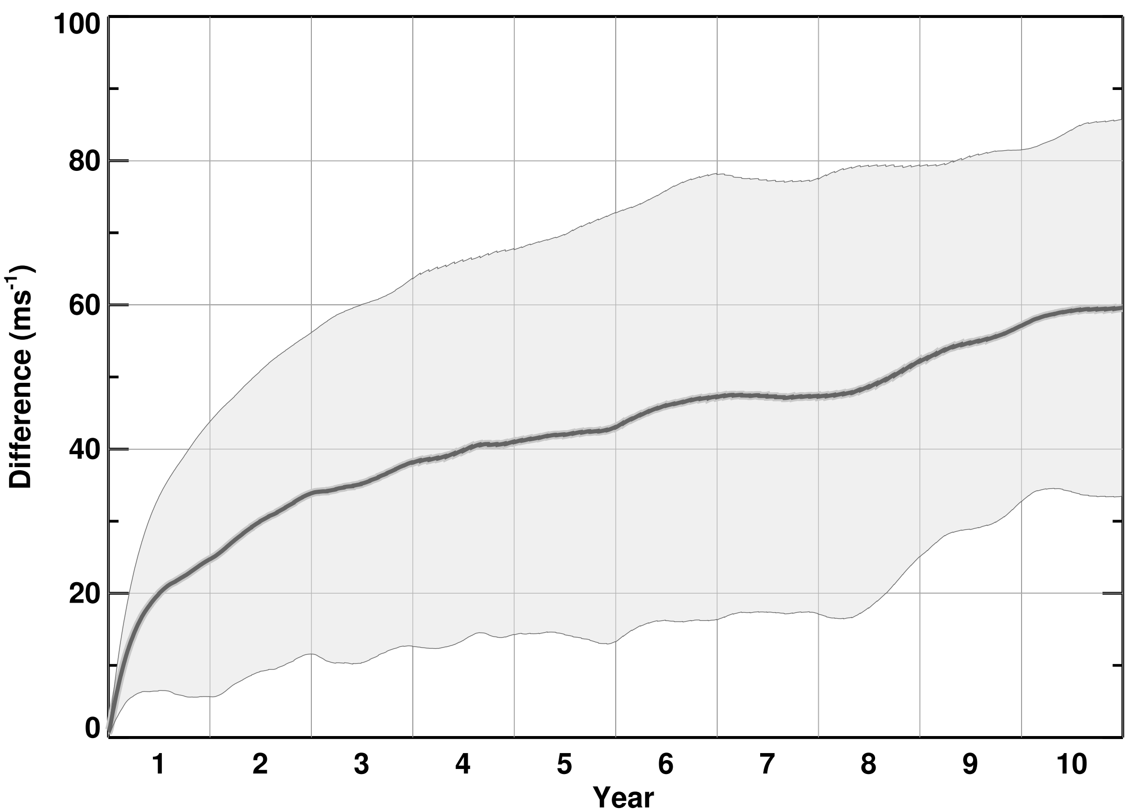

Figure 4. Averaged difference error (heavy gray curve) and standard deviation (light gray curves) between QBO phase propagation model initialized monthly from 1980–2018 and MERRA2.

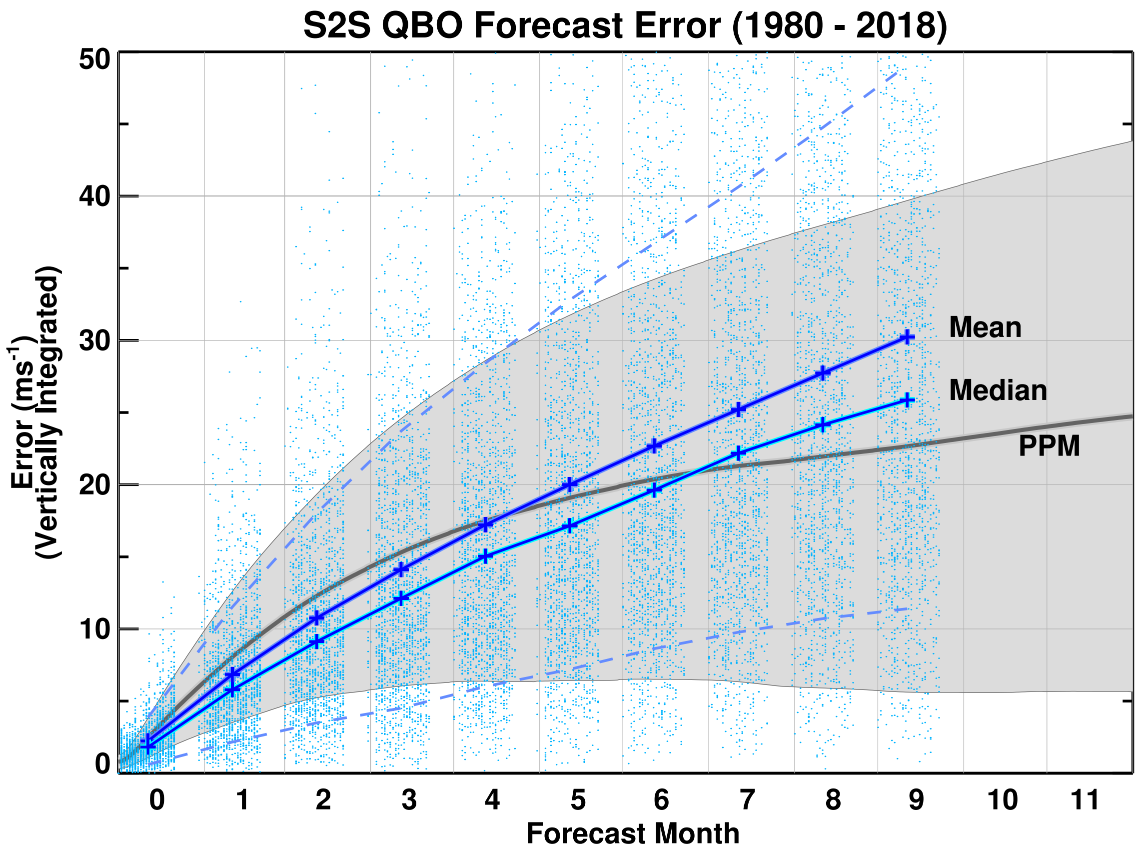

Figure 5. S2S forecast vector amplitude error (m/s) based on 1,835 9-month forecasts from 1980-2018: monthly mean (dark blue), standard deviation (dashed), monthly median (light blue) values, and individual monthly forecast values (light blue points). Also shown are the mean (dark gray) and standard deviation region (light gray) of the PPM as in Fig. 4. Note that the zero labeled month includes less than a full month as the S2S initialization starts before the start of the first full month.

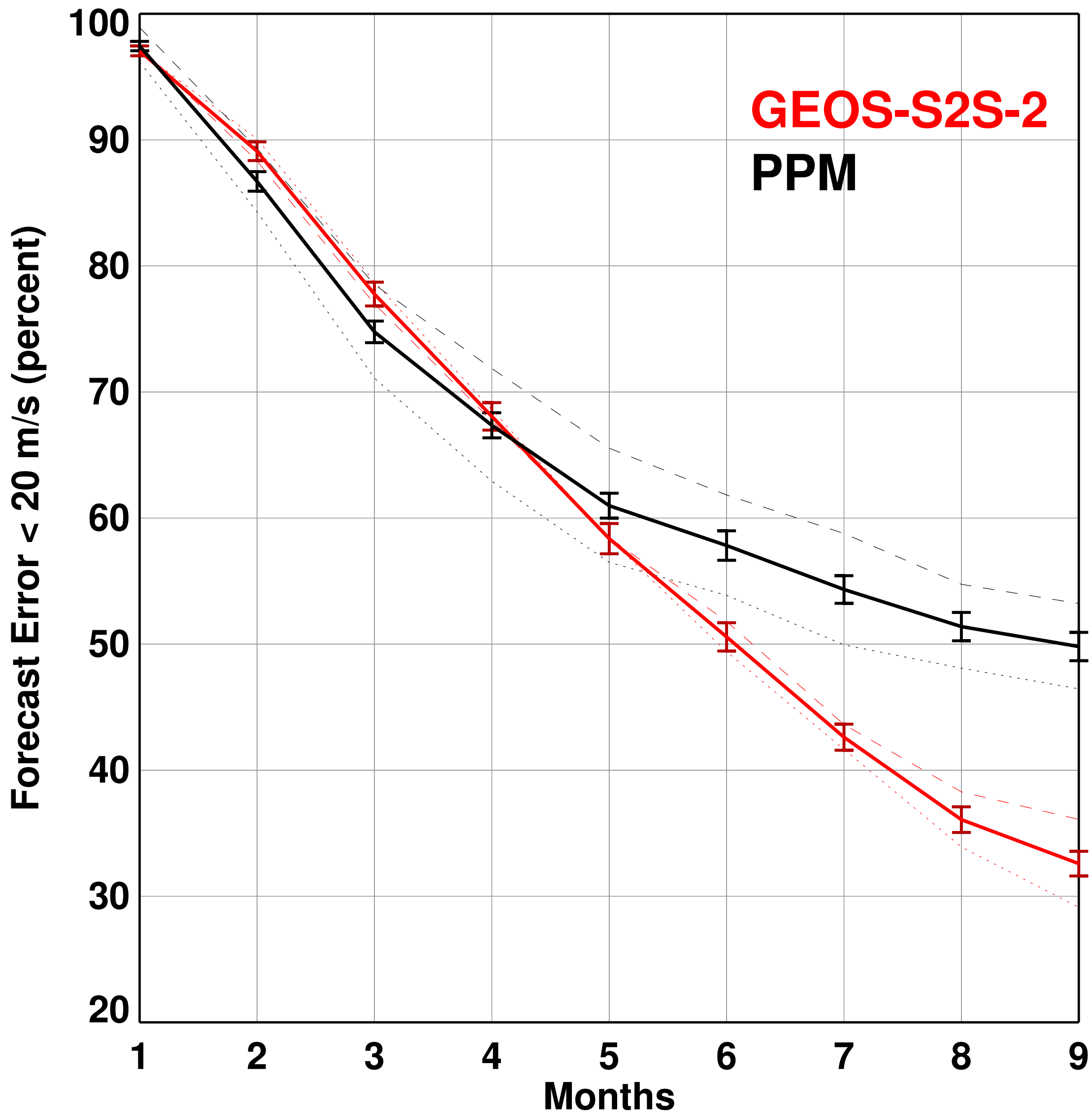

Figure 6. Percent of forecasts with the error less than 20 ms^{-1} as a function of forecast length (months) for GEOS-S2S (red) and the PPM (black) based on 1,835 forecasts initialized over the years 1981–2018. The error bars denote the standard deviation calculated when half the forecasts are randomly selected. The dashed and dotted curves show results for the years 1981–1999 and 2000–2018 respectively.

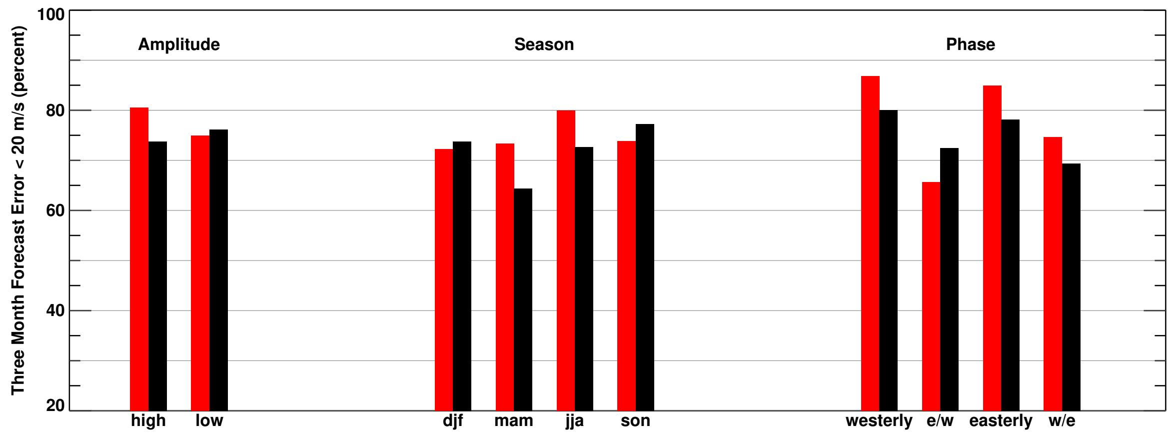

Figure 7. Percent of forecasts with the error less than 20 ms^{-1} for three month forecasts for S2S (red) and the PPM (black) sorted by initial amplitude, season, and phase.

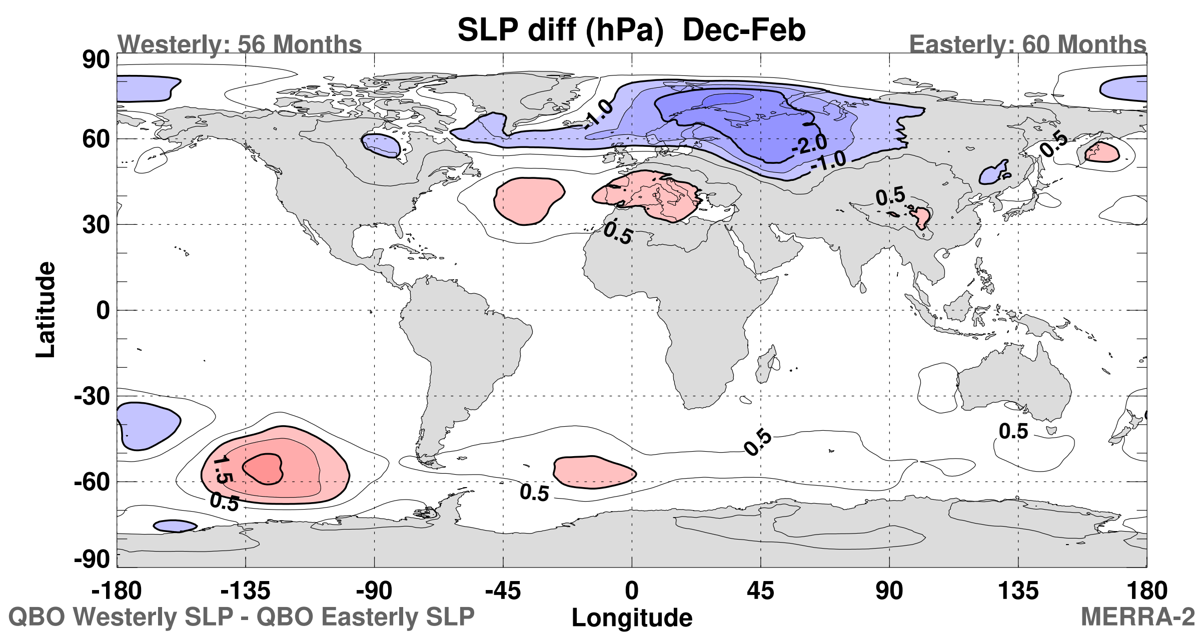

Figure 8. The MERRA-2 derived sea level pressure difference when composited by westerly and easterly QBO winds at 30 hPa during NH winter months (December, January, and February). The contour interval is 0.5 hPa. The zero contour is not plotted.

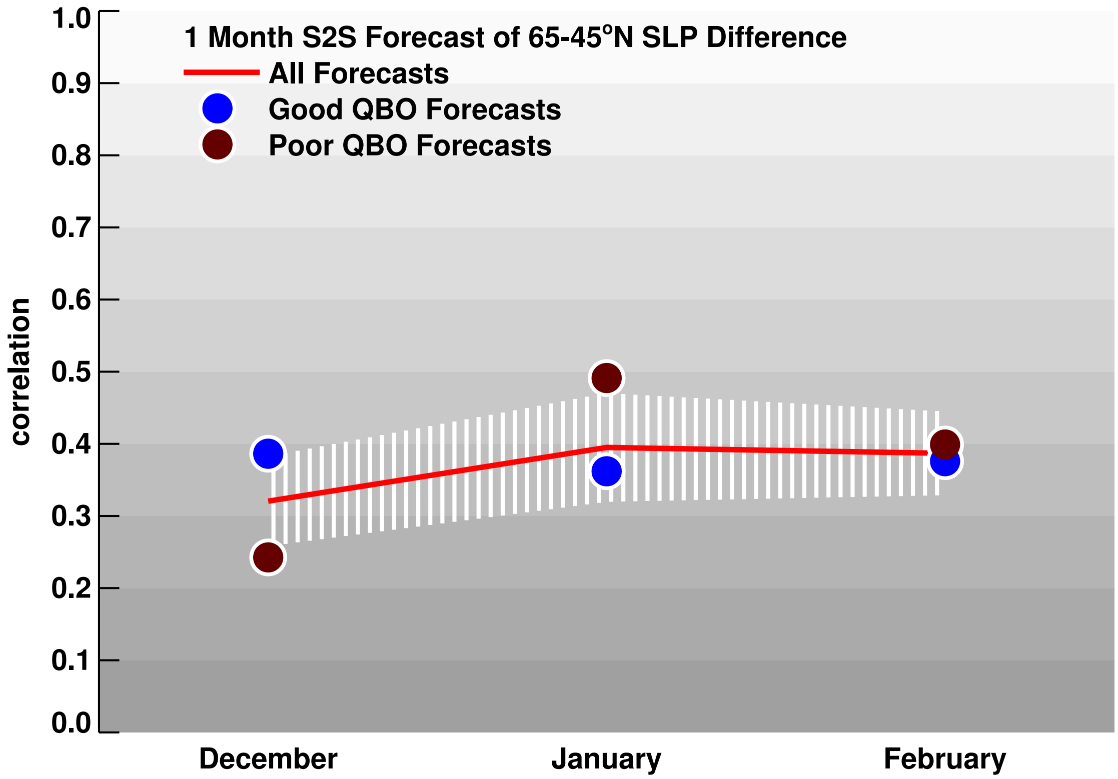

Figure 9. The correlation between MERRA-2 analyses and one month S2S retrospective forecasts of the sea level pressure difference between (0°E, 65°N) and (0°E, 45°N) valid for December, January, and February (red curve). The blue and brown filled circles show the correlation sorted by S2S QBO one month forecast errors below and above the median value respectively. The vertical white lines denote the standard deviation when half of the S2S forecasts are randomly selected.

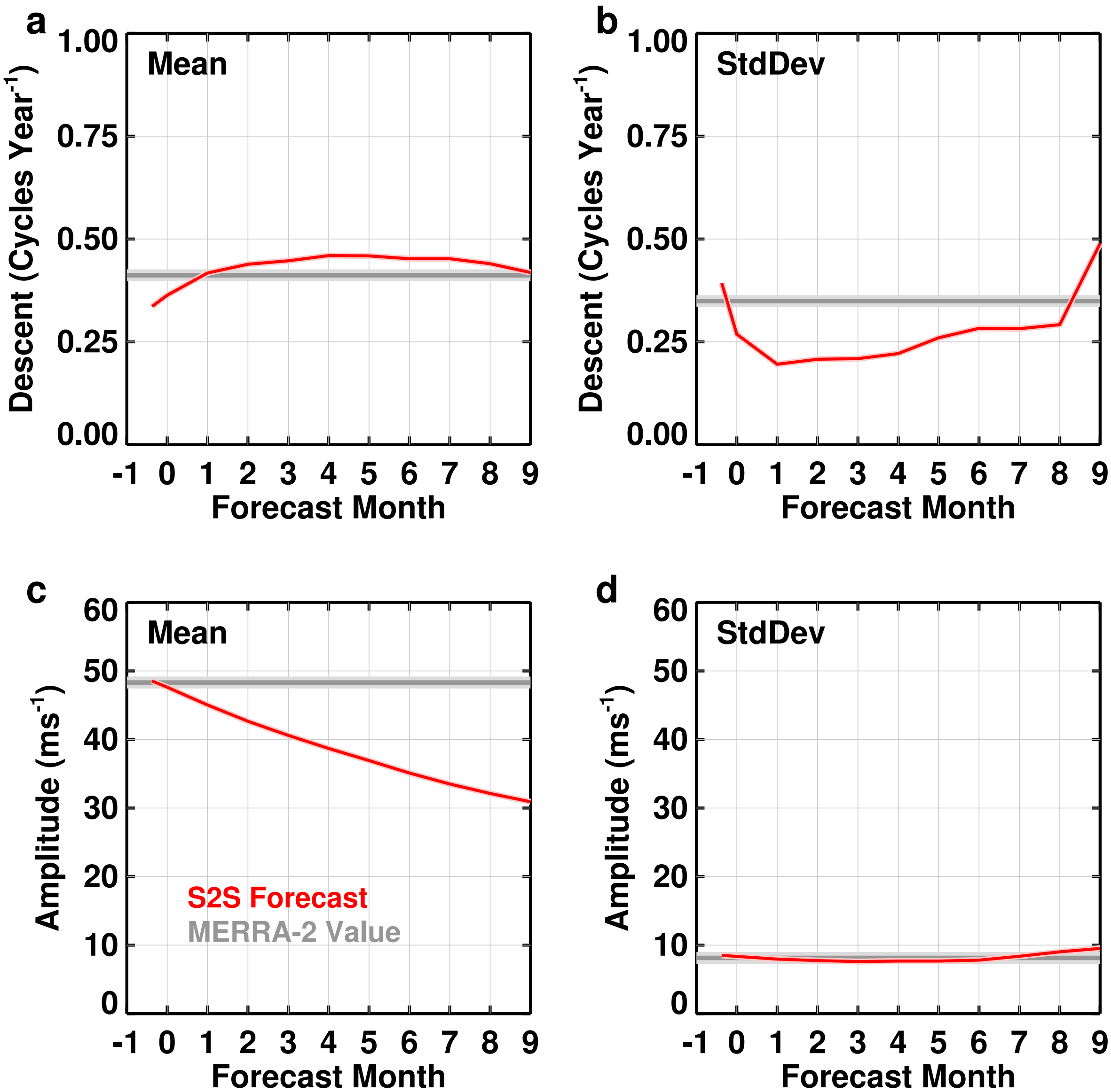

Figure 10. S2S 9-month forecast average QBO descent rate (cycles/year): a) mean and b) standard deviation and QBO amplitude (m/s): c) mean and d) standard deviation as a function of forecast lead time (months). The gray horizontal lines denote the corresponding MERRA-2 average values.

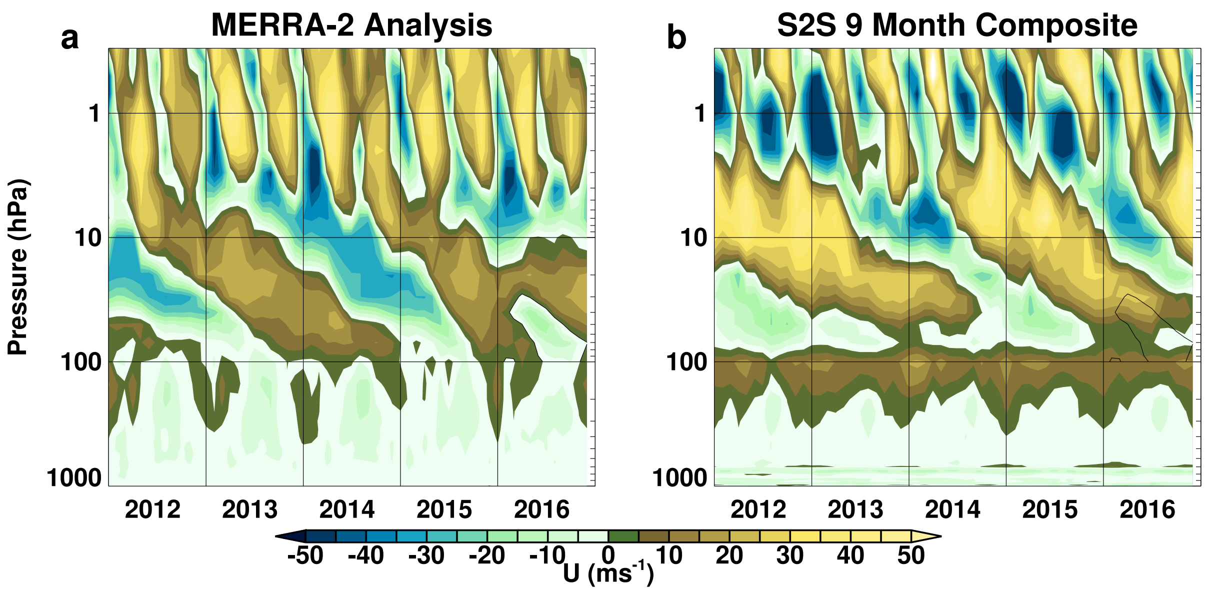

Figure 11. The monthly averaged, 10°S–10°N, zonal mean zonal wind (ms^{-1}) for a) MERRA-2 Analysis, and b) composite of S2S 9-month forecasts. The S2S values are also averaged over the four forecasts initialized each month. The monthly fields are plotted as a function of time (years) and pressure (hPa).

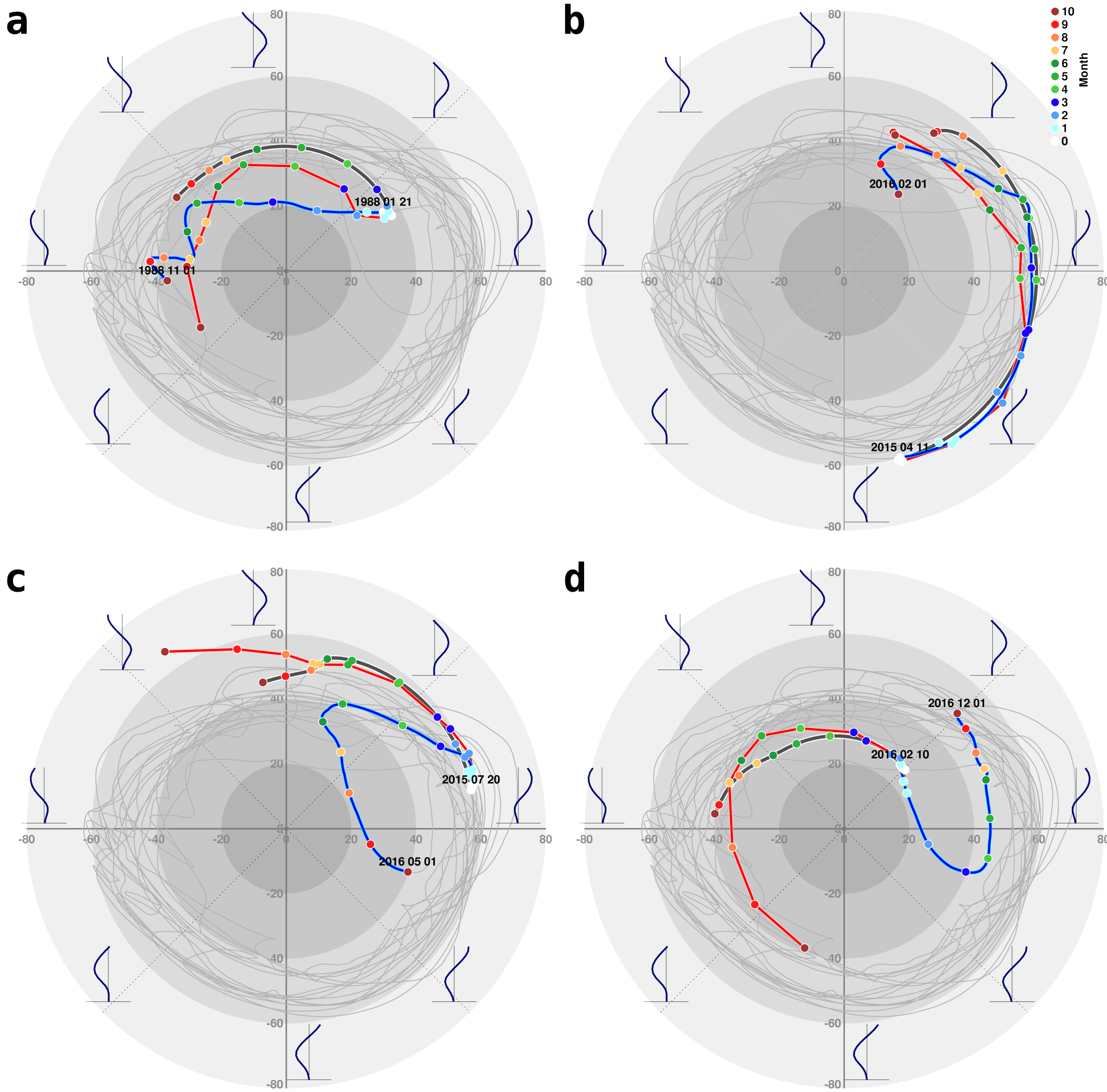

Figure 12. QBO PCs one and two derived from MERRA-2 analyses, S2S retrospective forecasts, and PPM forecasts (blue, red, and black curves respectively) for initial times: a) 21 January 1988, b) 11 April 2015, c) 20 July 2015, and d) 10 February 2016. The color filled circles denote the start of corresponding months in the MERRA-2 analyses and S2S retrospective forecasts. The gray curve shows the MERRA-2 result for the QBO evolution over the full 1980-2019 period (and so the blue curves each cover 9 months of the gray curve)

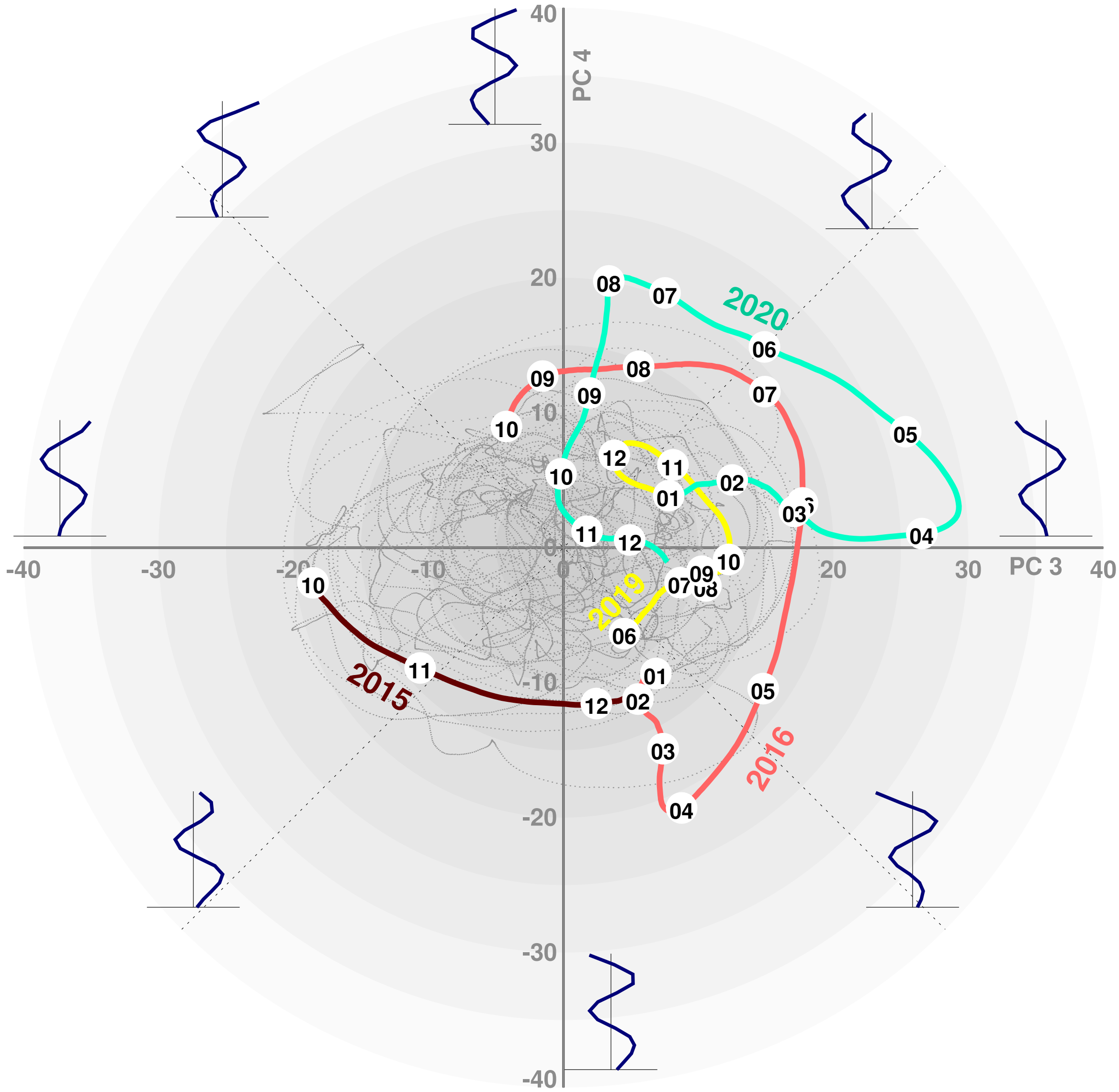

Figure 13. Same as Fig. 1 for PC3 vs PC4.